SIMULTANEOUS INVERSION OF RECEIVER FUNCTIONS, MULTI-MODE DISPERSION, AND TRAVEL-TIME TOMOGRAPHY FOR LITHOSPHERIC STRUCTURE BENEATH THE MIDDLE EAST AND NORTH AFRICA

Charles J. Ammon,[1] Robert B. Herrmann,[2] Michael E. Pasyanos,[3] William R. Walter,[3] Minoo Kosarian[1]

Penn State University,[1] Saint Louis University,[2] Lawrence Livermore National Laboratory[3]

ABSTRACT

We report on our initial investigations into the seismic structure of the lithosphere in the Middle East and North Africa (MENA) using surface waves and receiver functions. We have initiated the collection of prior work in the region and computing receiver functions for use in the joint inversion. Critical to the joint inversion is surface-wave dispersion information localized to approximately the same region sampled by receiver functions. We continue to improve our surface wave dispersion model of Western Eurasia and North Africa. We have developed group velocity maps at 2 degree resolution for both Love and Rayleigh waves from 10-100 seconds period. The model shows excellent relationship to tectonic structure and group velocity variations correlate well with orogenic zones, cratons, sedimentary basins, and rift zones. We have recently implemented a variable-resolution tomography and have pushed the resolution of the model down to 1 degree in areas with sufficient density sampling. We plan to present information on the complexity of receiver structure at many permanent sites in the region and several illustrative inversions for lithospheric structure. We have examined receiver functions at over 40 MENA stations and have inverted a number using dispersion measurements from global tomographic models. We will present a comparison of crustal thickness and Poisson's ratio estimates for the crust beneath these stations. Other work on the combination of additional observations (body-wave travel times, higher-mode observations, surface-wave polarization information) is planned for the future stages of the project, but we include illustrations outlining our ideas for the use of these data to help further constrain the seismic structure of the lithosphere.

OBJECTIVES

Our objectives are the construction of shear-velocity profiles for regions surrounding broad-band seismic stations throughout the Middle East, central and north Africa, and parts of western Europe. Application of the technique in the MENA region provides an opportunity to revise models of the crust and upper mantle structure throughout the region and to exploit the global and regional work of previous seismic verification research (*e.g.* Pasyanos *et al.*, 2001; Ritzwoller & Levshin, 1998, Larson *et al.*, 2001). The resulting shear-velocity models provide a single structure consistent with a range of observations that can be tested as a tool for the construction of mode isolation filters to help improve surface-wave magnitude estimates. We also plan to explore the possibility of adding additional data to our inversions of receiver functions and surface-wave dispersion estimates. The diverse seismic activity throughout the region will facilitate cross-validation of the mode isolation filters with simple empirical filters constructed using larger events with adequate signal-to-noise ratios.

Estimating Subsurface Shear Velocities

Subsurface geology generally has a broad "wavenumber" spectrum containing sharp, or high-wavenumber, changes in velocity near Earth's major geologic boundaries and smooth low-wavenumber variations in regions of relatively uniform geologic structure. Access to the full spectrum of earth structure requires that we exploit signals that span a wide frequency range and that are sensitive to the entire spectrum of heterogeneity. Surface-waves, travel times, and direct-wave amplitudes, for example, are sensitive to smooth variations in earth structure; reflected and converted waves are sensitive to velocity contrasts. Combining seismic data in joint inversions is an obvious approach to improve estimates of earth structure. To successfully combine data in an inversion, we must insure that all the data are sensitive to the same (or related) physical quantities and that they sample or average structure over comparable length scales. Recent advances in surface-wave tomography have provided an opportunity to combine localized surface-wave dispersion estimates with other data such as P- and S-wave receiver functions. Ammon and Zandt (1993) used surface-wave dispersion observations to try and distinguish between competing models of the Mojave desert, but Ozalaybey *et al.*, (1997) pioneered a formal, joint inversion of these data. They nicely illustrated the value of even a limited band of dispersion values to help reduce the trade-off between crustal thickness and velocity inherent in receiver function analyses. Specifically, they used Rayleigh-wave phase velocities in the 20-25 second period range to help produce stable estimates of crustal thickness in the northern and central Basin & Range. The limited bandwidth did not permit resolution of details in the crust and they limited their inversion (or at least their interpretation) to depths above 40 km. More recent authors have exercised the approach and combined the data with additional *a priori* model constraints (Du and Foulger, 1999; Julia *et al.*, 2000). Recent accomplishments in global and regional tomography now provide a more complete band of dispersion measurements to combine with receiver functions that allow us to improve the resolution of earlier works.

Surface-wave dispersion measurements are sensitive to broad averages, or low wavenumber components of earth structure. They provide valuable information on the absolute seismic shear velocity but are relatively insensitive to sharp, high-wavenumber velocity changes. Generally surface-wave inversions must be constrained using a particular layer parameterization (*e.g.* near-surface, upper-crust, lower crust, mantle lid, deep mantle), resemble an *a priori* model, or substantially smoothed to stabilize earth-structure estimation. Despite these drawbacks, surface-wave dispersion values contain important constraints on the subsurface structure, and the general increase in depth sensitivity with depth allows an intuitive understanding of their constraints on structure. Additionally, modeling dispersion values facilitates a broadband inversion by reducing the dominance of airy phases, which pose problems when constructing broad-band misfit norms to model seismograms directly. Perhaps most important for our application is the ability to localize Earth's dispersion properties using seismic tomography. The idea is now well established and global dispersion models exist for a broad range of frequencies (*e.g.* Larson and Ekstrom, 2001; Stevens *et al.*, 2001). The localization of dispersion allows us to isolate the variations in properties spatially and global models of surface-wave dispersion exist and are readily available for application to other studies such as the proposed work.

Receiver functions are time series computed from three-component body-wave seismograms, that show the relative response of Earth structure near the receiver (*e.g.* Langston, 1979). Source, near-source structure, and mantle propagation effects are removed from the seismograms using a deconvolution that sacrifices P-wave information for

the isolation of near-receiver effects (Langston, 1979; Owens *et al.*, 1984; Ammon, 1991; Cassidy, 1992). Receiver function waveforms are a composite of P-to-S (or S-to-P) converted waves that reverberate within the structure near the seismometer. Modeling the amplitude and timing of those reverberating waves can supply valuable constraints on the underlying geology. In general, the receiver functions sample the structure over a range of 10's of kilometers from the station in the direction of wave approach (the specific sample width depends on the depth of the deepest contrast). Stations sited near geologic boundaries can produce different responses for different directions. Recent innovations in receiver function analysis include more detailed modeling of receiver function arrivals from sedimentary basin structures (*e.g.* Clitheroe *et al.*, 2000), anisotropic structures (*e.g.* Levin and Park, 1997; Savage 1998), estimation of Poisson's ratio (*e.g.* Zandt *et al.*, 1995; Zandt and Ammon, 1995; Zhu and Kanamori, 2000, Ligorría, 2000), reflection-like processing of array receiver functions (*e.g.* Chevrot and Girardin, 2000; Ryberg and Weber, 2000) and joint inversions (*e.g.* Ozalaybey *et al.*, 1997; Du and Foulger, 1999; Julia *et al.*, 2000).

Our joint inversion method is similar to that of Ozalaybey *et al.* (1997) except that we use jumping, smoothness, and constraints to include as much *a priori* information into the inversion as is available. We combine the receiver function and surface-wave observations into a single algebraic equation and account for their different physical units and equalize their importance in the misfit norm by weighting each dataset by an estimate of the uncertainty in the observations and the number of data. We also append smoothness constraints and *a priori* model constraints on the deepest part of the model. Although we cannot resolve fine details in the deep upper mantle, these regions can impact our results since surface-wave dispersion values at intermediate and longer periods are somewhat sensitive to this deeper structure. We believe that it is important to have a reasonable basement structure so that our results are more consistent with global models. We extend our models to about 500-700 km to insure this consistency. The resulting inversion equations are

$$
\begin{bmatrix} \sqrt{\dfrac{p}{w_s^2}}\mathbf{D}_s \\ \sqrt{\dfrac{q}{w_r^2}}\mathbf{D}_r \\ \sigma\Delta \\ \mathbf{W} \end{bmatrix} \cdot \mathbf{m}_{i+1} = \begin{bmatrix} \sqrt{\dfrac{p}{w_s^2}}\mathbf{r}_s \\ \sqrt{\dfrac{q}{w_r^2}}\mathbf{r}_r \\ 0 \\ 0 \end{bmatrix} + \begin{bmatrix} \sqrt{\dfrac{p}{w_s^2}}\mathbf{D}_s \\ \sqrt{\dfrac{q}{w_r^2}}\mathbf{D}_r \\ 0 \\ 0 \end{bmatrix} \cdot \mathbf{m}_i + \begin{bmatrix} 0 \\ 0 \\ 0 \\ \mathbf{W} \end{bmatrix} \cdot \mathbf{m}_a \qquad (1)
$$

where $\mathbf{p}$, $\mathbf{q} = 1 - \mathbf{p}$, σ, and $\mathbf{W}$ are weights that control the relative importance of receiver functions, dispersion values, smoothness, and *a priori* model constraints in the norm minimized during the inversion. The data comprise the vectors $\mathbf{r}_s$ and $\mathbf{r}_r$, and the partial derivatives fill the matrices $\mathbf{D}_r$ and $\mathbf{D}s$. The matrix Δ is a finite-difference stencil that "computes" model roughness, and the matrix $\mathbf{W}$ is a layer-dependent weight that is used to insure the model blends smoothly into the *a priori* model, $\mathbf{m}_a$, at depth. The values of $\mathbf{w}_s$ and $\mathbf{w}_r$ are equal to the product of the number of points in the dispersion curve and receiver functions and the variance of the observations.The second term on the right is added to create the "jumping" inversion scheme (*e.g.* Constable *et al.*, 1987; Ammon *et al.*, 1990) and allows us to solve for (and constrain) the shear-velocity models as opposed to shear-velocity correction vectors. Equation (1) is solved in a least-squares sense for the model, $\mathbf{m}_{i+1}$, starting with an initial model $\mathbf{m}_0$. The procedure generally converges in a few iterations.

Estimating Receiver Functions

When the data are high-quality and the receiver structure is not too complex, the choice of a deconvolution procedure does not make much difference. However, when the noise in the seismograms is substantial, or the receiver structure is complex, different deconvolution approaches have strengths and weaknesses. We will compute receiver functions using the iterative time-domain deconvolution procedure described by Ligorría and Ammon (1999). We prefer the iterative approach, which is based on the Kikuchi and Kanamori (1982) source-time function estimation algorithm, for several reasons. First, in the iterative approach the receiver function is constructed by a sum of Gaussian pulses which produces a flat spectrum at the longest periods. The flat long-period spectrum can be viewed as *a priori*

information that helps reduce side-lobes that may result of spectral or singular-value truncation stabilization procedures. The reduction of side-lobes eases the interpretation and helps stabilize "low-frequency" receiver functions. Second, the iterative approach constructs a causal receiver function, which is what we expect in all cases of reasonable earth structure. This is a subtle difference from spectral techniques (*e.g.* Langston, 1979; Park and Levin, 2000) which can always introduce a component to the signal before the P-wave. The acausal component of the spectral signal may be small, but still important to the satisfaction of the convolutional model that defines a receiver function, *i.e.:*

$$\mathbf{R(t)} \ = \ \mathbf{Z(t)} * \mathbf{E_R(t)} \,. \tag{2}$$

In equation (2), $\mathbf{R(t)}$ and $\mathbf{Z(t)}$ are the radial and vertical seismograms, and $\mathbf{E_R(t)}$ is the radial receiver function (a similar equation holds for the transverse component). The point is that even when the receiver function estimation is unstable, spectral deconvolutions may satisfy (2) quite well. The iterative time-domain approach, which can be restricted to produce the best *causal* solution, may not always satisfy (2). Experienced modelers have always been able to identify failed receiver functions, but the misfit to (2) available from iterative deconvolutions provides quantitative information that can be used when stacking signals, or in extreme cases, to discard obviously failed deconvolutions. In our case we find using a threshold cut-off of 80-90% of the radial power fit allows us to quickly discard poorly constrained deconvolution results, enabling an efficient and objective select of the data to include in further analysis.

RESEARCH ACCOMPLISHED

Receiver Function Computation

The first step in the project is the selection of target stations and the computation of receiver functions at those stations. To begin, we have a selected a subset of permanent stations that have relatively long recording histories and thus will have substantial data already available. More recently installed stations and operating temporary stations will be added later in the project. Data processed at the time this report was written are shown in Figure 1. We plan to include all available temporary and permanent stations within central and norther Africa, the Middle East, and parts of Europe. So far we have investigated 69 stations, 36 in Africa, 34 in the Middle East, and 24 stations in southern Europe.

Poisson's Ratio and Crustal Thickness Estimation

As a first step in the receiver function analysis we use the receiver function stacking method of Zhu and Kanamori (2000) to estimate the crustal thickness and Vp/Vs velocity ratio (or Poisson's ratio). The stacking method makes a rather limiting assumption of a uniform crust but the analysis provides good estimates of these quantities when the structure is relatively simple. The estimated values of Poisson's ratios can be used in subsequent inversions which require some assumed value of bulk crustal Poisson's ratio. We summarize the results so far in Figure 2. If a station is shown twice, that indicates that we observed significant azimuthal variations (which may indicate a likely failure of this simple imaging approach). Ignoring obvious outliers, we see an overall trend suggesting a decrease in Poisson's ratio (Vp/Vs) with increasing crustal thickness. The trend is primarily cause by results for stations in southwestern Asia and the trend is absent in results for stations sampling Africa and southern Europe. The fact that two of three geographic clusters do not show the feature suggest it is not an artifact of the method. The pattern may still be "coincidence" since the data from southwestern Asia span a large and the lowest values are unusually low, perhaps a result of lateral heterogeneity unaccounted for in the method. Still, all are located in the zone of plateaus and collision-related uplifts and more analysis is need to investigate the trend's validity and its potential explanations. Crustal thickness agree in general with the global crustal model 2.0, but at times the differences are significant (greater than 5 km). The median difference between the global model and our results is 0 km, the median absolute difference is 3 km. The numbers agree more closely when we rank our estimates using the complexity of the observed receiver functions.
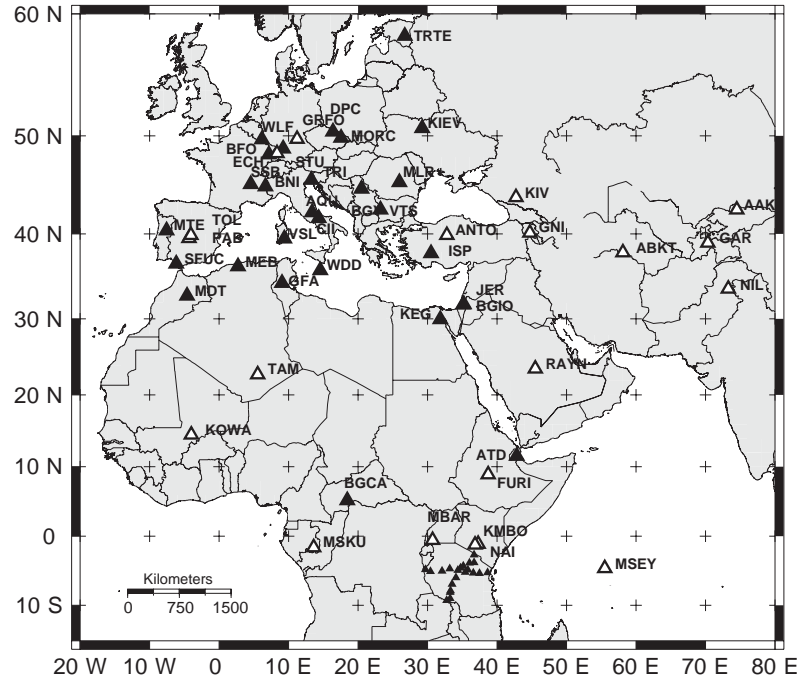
Figure 1. Stations for which we have computed receiver functions (as of the date of this report). The eventual target stations include all available permanent and temporary three-component seismic stations. Shaded symbols indicate stations analyzed since the last review.
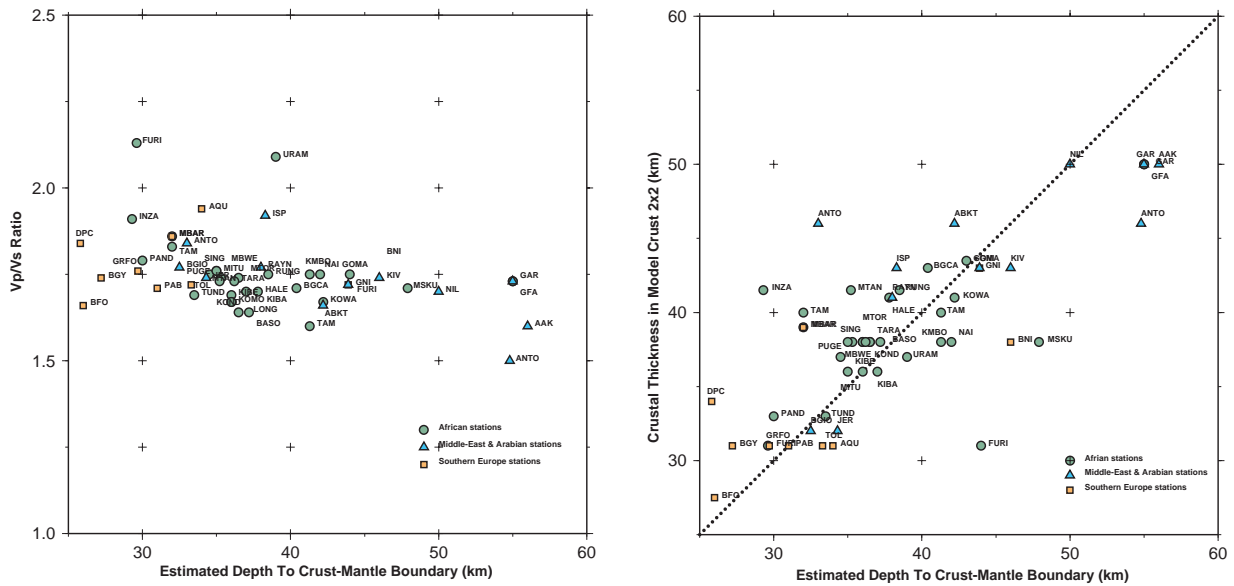

Figure 2. Variation of Vp/Vs ratio with crustal thickness and comparison of crustal thickness estimated with receiver functions versus values from crustal model 2.0.

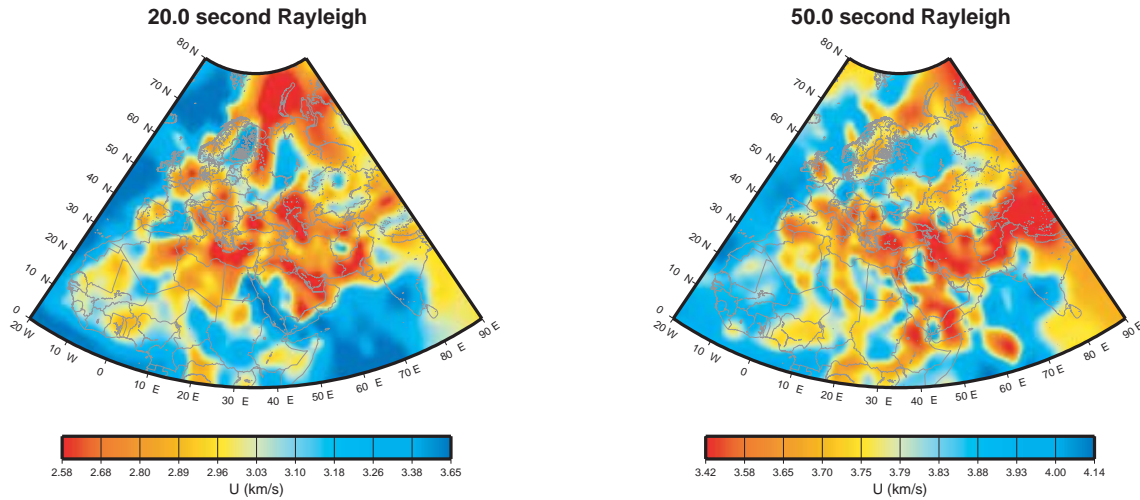**20.0 second Rayleigh**   **50.0 second Rayleigh**

Figure 3. Tomographic imaging results for the Middle-East, North Africa, and western Europe. The upper diagram shows the lateral group velocity variations in 20-second period Rayleigh waves, the lower 50-second period Rayleigh waves.

Tomographic Imaging of Group-Velocity Variations

We have performed a large-scale study of surface wave group velocity dispersion across Western Eurasia and North Africa (Pasyanos, 2002). This study expands the coverage area northwards relative to previous work (Pasyanos *et al.*, 2001), which covered only North Africa and the Middle East. As a result, we have increased by about 50% the number of seismograms examined and group velocity measurements made. We have now made good quality dispersion measurements for about 10,000 Rayleigh wave and 6,000 Love wave paths, and have incorporated measurements from several other researchers into the study. We use a conjugate gradient method to perform a group velocity tomography.

We have improved our inversion from the previous study by adopting a variable smoothness (Pasyanos, 2002). This technique allows us to go to higher resolution where the data allow without producing artifacts. Our current results include both Love and Rayleigh wave inversions across the region for periods from 10-100 seconds. Figure 3 shows inversion results for Rayleigh waves at periods of 20 and 50 seconds. Short period group velocities are sensitive to slow velocities associated with large sedimentary features such as the Russian Platform, Mediterranean Sea, and Persian Gulf. Intermediate periods are sensitive to differences in crustal thickness, such as those between oceanic and continental crust or along orogenic zones. At longer periods, we find fast velocities beneath cratons and slow upper mantle velocities along rift systems and the Tethys Belt.

An Example Combined Inversion, Station PUGE, Tanzania

We illustrate the ideas with an example. In Figure 4 we present the results of the inversion of PUGE receiver functions with the Rayleigh-wave group-velocity dispersion values from Pasyanos and Walter (2002) combined with phase velocities digitized from Weeraratne *et al* (2003). The fit to the Pasyanos and Walter (2002) dispersion curve is very good and the general fit to the phase-velocities is good. The phase velocities are slightly under-predicted for the shorter periods and over-predicted for the longest periods. The long-period over-prediction is a result of our constraints that the deepest part of the model match that of PREM. Relaxing that assumption would allow the low velocities to extend deeper that 220 km and reduce the deepest average shear-velocity to match the phase velocity. The difference at the shorter periods represents a fundamental difference between the group and phase-velocities. One explanation may be the smoothing of the group velocities has resulted in an artificially lower estimate - very slightly inconsistent with the phase velocities. The receiver functions are very well modeled and produce the relatively smooth crust-mantle transition and crustal thickness (provided with the absolute velocity information from
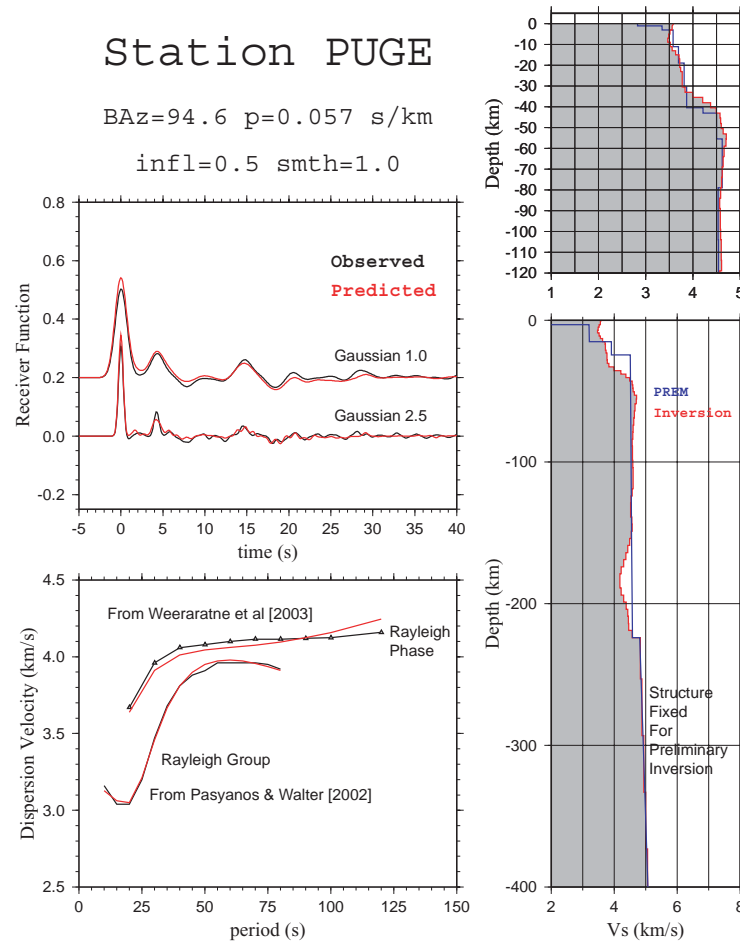
39

Figure 4. Inversion results for station PUGE using dispersion curves from Pasyanos and Walter (2002) & Weereratne et al., (2003). The back azimuth and ray parameter of the incoming P-wave are shown at the top. The influence parameter was 0.5, which balances the weight between the receiver functions and dispersion values, and the smoothness weight was 1.0. The observed and predicted receiver functions in two bandwidths are shown in the upper left, the observed and predicted dispersion curves in the lower left, and the resulting models are shown on the right. The deep structure is constrained to transition smoothly into the PREM - the data have little sensitivity for detailed absolute velocities below approximately 100-150 km. These velocities are earth-flattened by default since we use flat-earth codes to perform the analyses.

the surface-wave information).The model has a relatively simple crust, consistent with earlier results, and the crust-mantle transition about 7.5 km thick (this could be an intermediate layer at the base of the crust). The mantle structure includes a lid with a thickness of approximately 100 km underlain by a region of low velocities. These velocities are low compared with other shields - consistent with the results of Weeraratne et al (2003). Although the lid is fast at shallow depths, consistent with regional propagation (e.g. Nyblade and Brazier, 2002; Langston et al., 2002) the model lid is also thinner than usual for an Archean shield.

CONCLUSIONS AND RECOMMENDATIONS

Our work is proceeding nicely and most of the permanent stations have been imaged. We are also working with other groups to secure and image structures beneath several more sites in northeastern Africa. We have a few more permanent stations to analyze. We are moving from the initial data collection and preliminary analysis phase into a more expansive interpretation and assessment stage.

REFERENCES

Ammon, C.J., G.E. Randall, and G. Zandt (1990), On the non-uniqueness of receiver function inversions, *J. Geophys. Res.*, 95, 15303-15318.

Ammon, C.J. (1991), The isolation of receiver effects from teleseismic P waveforms, *Bull. Seism. Soc. Am.*, 81, 2504-2510.

Ammon, C. J., and G. Zandt (1993), The receiver structure beneath the southern Mojave Block, *Bull. Seism. Soc. Am.*, 83, 737-755.

Cassidy, J.F., Numerical experiments in broadband receiver function analysis, *Bull. Seismol. Soc. Am.*, 82, 1453-1474, 1992.

Chevrot, S., and N. Girardin (2000), On the detection and identification of converted and reflected phases from receiver functions, *Geophys. J. Int.*, 141 (3), 801-808.

Clitheroe, G., O. Gudmundsson, and B.L.N. Kennett (2000), Sedimentary and upper crustal structure of Australia from receiver functions, *Australian Journal of Earth Sciences*, 47 (2), 209-216.

Constable, S.C., R.L. Parker, and C.G. Constable (1987), Occam's inversion: A practical algorithm for generating smooth models from electromagnetic sounding data, *Geophysics*, 52, 289-300.

Du, Z.J. and G.R. Foulger (1999), The crustal structure beneath the northwest fjords, Iceland, from receiver functions and surface waves, *Geophys. J. Int.*, 139, 419-432.

Julia, J., C. J. Ammon, R. B. Herrmann, and A. M. Correig (2000), Joint Inversion of receiver function and surface-wave dispersion observations, *Geophys. J. Int.* 143, 99-112.

Kikuchi, M., and H. Kanamori, Inversion of complex body waves (1982), *Bull. Seism. Soc. Am.*, 72, 491-506, 1982.

Langston, C.A. (1979), Structure under Mount Rainier, Washington, inferred from teleseismic body waves, *J. Geophys. Res.*, 84, 4749-4762.

Larson, E. W. F. and G. Ekstrom (2001), Global Models of Group Velocity, *Pure and Applied Geophys.*, 158, 1377-1399.

Levin, V., and J. Park (1997), Crustal anisotropy in the Ural Mountains from teleseismic receiver functions, *Geophysical Research Letters*, 24 (11), 1283-1286.

Ligorría, J.P. (2000), An Investigation of the Crust-Mantle Transition Beneath North America and the Bulk Composition of the North American Crust, *Ph.D. Thesis, Saint Louis University*, 261 pages.

Ligorría, J.P. and C. J. Ammon (1999), Iterative deconvolution and receiver function estimation, *Bull. Seismol. Soc. Am.*, 89, 1395-1400.

Myers, S.C., and S.L. Beck (1994), Evidence for a local crustal root beneath the Santa Catalina metamorphic core complex, Arizona, *Geology*, 22, 223-226.

Owens, T.J., G. Zandt, and S.R. Taylor (1984), Seismic evidence for an ancient rift beneath the Cumberland Plateau, Tennessee: A detailed analysis of broadband teleseismic P waveforms, *J. Geophys. Res.*, 89, 7783-7795.

Ozalaybey, S., M.K. Savage, A.F. Sheehan, J.N. Louie, and J.N. Brune (1997), Shear-wave velocity structure in the northern Basin and Range Province from the combined analysis of receiver functions and surface waves, *Bull. Seismol. Soc. Am.*, 87, 183-199.

Park, J., and V. Levin (2000), Receiver functions from multiple-taper spectral correlation estimates, *Bull. Seismol. Soc. Am.*, 90 (6), 1507-1520.

Pasyanos, M.E., W.R. Walter, and S.E. Hazler (2001), A Surface wave dispersion study of the Middle East and North Africa for Monitoring the Comprehensive Nuclear-Test-Ban Treaty, *Pure and Applied Geophys*, 158, 1445-1474.

Pasyanos, M.E., and W.R. Walter, Crust and upper-mantle structure of North Africa, Europe and the Middle East from inversion of surface waves, Geophys. J. Int., 149, 463-481, 2002.

Pasyanos, M.E. (2002), A Variable-resolution Surface Wave Dispersion Study of Western Eurasia and North Africa, submitted to *Journal of Geophysical Research*.

Ritzwoller, M. H. and A. L. Levshin (1998), Eurasian surface wave tomography: Group velocities, *J. Geophys. Res., 103*, 1839-1878.

Ryberg, T., and M. Weber (2000), Receiver function arrays; a reflection seismic approach, *Geophys. J. Int.*, 141 (1), 1-11.

Sandvol, E., D. Seber, A. Calvert, M. Barazangi (1998), Grid search modeling of receiver functions: Implications for crustal structure in the Middle East and North Africa, *J. Geophys. Res.*,103, 26,899-26,917.

Savage, M.K. (1998), Lower crustal anisotropy or dipping boundaries? Effects on receiver functions and a case study in New Zealand, *J. Geophys. Res.*, 103 (7), 15,069-15,087, 1998.

Stevens, J. L. and K. L. McLaughlin (2001), Optimization of Surface Wave Identification and Measurement, *Pure and Applied Geophys*., 158, 1547-1582

Su, W., R. L. Woodward, and A. M. Dziewonski (1994), Degree 12 model of shear velocity heterogeneity in the mantle, *Nature*, 99, 6945-6980.

Weeraratne, D.S., D.W. Forsyth, K.M. Fischer, and A.A. Nyblade, Evidence for an upper mantle plume beneath the Tanzanian craton from Rayleigh wave tomography, *J. Geophys. Res.*, 2002JB002273R, 2003.

Zandt, G., and C. J. Ammon (1995), Continental Crustal composition constrained by measurements of crustal Poisson's ratio, *Nature*, 374, 152-154.

Zandt, G., S.C. Myers, and T.C. Wallace (1995), Crust and mantle structure across the Basin and Range-Colorado Plateau boundary at 37 degrees N latitude and implications for Cenozoic extensional mechanism, *J. Geophys. Res.*, 100 (6), 10,529-10,548.

Zhu, L., and H. Kanamori (2000), Moho depth variation in Southern California from teleseismic receiver functions, *J. Geophys. Res.*, 105 (2), 2969-2980.